Colloid and Polymer Science (2018) 296:1805–1816
https://doi.org/10.1007/s00396-018-4402-z

ORIGINAL CONTRIBUTION

Synthesis of nanoporous organic/inorganic hybrid materials with adjustable pore size

Y. Qawasmi[1] · P. Atanasova[2] · T. Jahnke[2] · Z. Burghard[2] · A. Müller[3] · L. Grassberger[3] · R. Strey[3] · J. Bill[2] · T. Sottmann[1]

Received: 5 March 2018 / Revised: 30 August 2018 / Accepted: 31 August 2018 / Published online: 14 September 2018

Abstract

Polystyrene (PS) nanofoams, prepared following the *nanofoams continuity inversion of dispersions* (NF-CID) principle, were utilized for the synthesis of nanoporous organic/inorganic hybrid materials. The pore size and morphology of the PS foams were found to depend on the NF-CID parameters: temperature, exposure time, and the expansion process. With this knowledge, PS foams with a pore size of 1 μm were mineralized with ZnO from a methanol precursor solution comprising zinc acetate dihydrate. Scanning electron microscopy (SEM) coupled with energy-dispersive X-ray (EDX) was used to characterize both the pure PS nanofoam and the hybrid material. The formation of a ZnO layer on the pore walls of the polymer foams was confirmed, while the general structure of the foam was retained. Uniaxial compression measurements revealed larger values of the *E* modulus and the yield stress for the porous PS/ZnO hybrid material compared to the pure polymer foam.

Keywords Supercritical carbon dioxide · Mineralization · Polystyrene nanofoams · Organic/inorganic hybrid materials · Hard template

Introduction

Organic/inorganic hybrid materials with their complex and often unusual features have numerous advanced functional applications in fields like energy, microelectronics, and optics [1]. The synthesis of such hybrids requires low-temperature methods especially when organic templates are used. These sensitive templates cannot withstand the harsh reaction conditions often used by conventional methods for the synthesis of functional inorganic materials. In comparison, the organisms in living nature produce minerals at ambient conditions through biomineralization [2]. This process leads to the fabrication of bio/inorganic composites. Hereby, the formation of the inorganic components is usually controlled by biotemplates in localized volumes (e.g., in the case of the formation of nacre). Within these confinements, the organisms govern the mineralization process and hence the morphology and orientation of the minerals through control of the precursor ions and mineral phases [3].

Inspired by biomineralization, organic/inorganic mesoporous hybrids can be synthesized with more technologically relevant materials like functional oxides making use of the mild reaction conditions of chemical bath deposition (CBD). Here, the samples are placed in a liquid deposition solution and mineralized at low temperatures below 100 °C. Importantly, control over the mineralization process resulting in the synthesis of inorganic particles with adjustable features (size, crystallinity, and polarity) can help to tune the properties of the corresponding organic/inorganic materials. Additionally, the combination of an organic and inorganic phase is considered to enhance the mechanical and chemical stability of the hybrid material (similar to nacre).

In this work, polymeric nanofoams were utilized as tailor-made templates for the synthesis of highly porous organic/inorganic hybrid materials. Because of their low gaseous heat conductivity, which is a consequence of the Knudsen effect [4], polymeric nanofoams are considered as insulation materials of the future [5]. Polymeric nanofoams beat aerogels, which are produced in a sol-gel process [6], because they are

✉ T. Sottmann
thomas.sottmann@ipc.uni-stuttgart.de

[1] Institute of Physical Chemistry, University of Stuttgart, Stuttgart, Germany

[2] Institute for Materials Science, University of Stuttgart, Stuttgart, Germany

[3] Institute of Physical Chemistry, University of Cologne, Cologne, Germany

suffering from the unavoidable time-consuming supercritical drying step [7]. Thin films of nanoporous foams (pore size < 100 nm) were produced via the saturation of thermoresponsive polymers (polyetherimide, polysulfone, and poly(methyl methacrylate)) with supercritical carbon dioxide ($scCO_2$) and the subsequent sudden expansion [8, 9]. However, this approach is inappropriate for an efficient production of nanomaterials due to long saturation times and high expansion rates.

Inspired by template strategies, in which $scCO_2$-in-monomer emulsions are rapidly expanded and polymerized to generate microcellular foams [10], some of us developed the *Principle of Supercritical Microemulsion Expansion* (POSME) [11, 12] and the *Nanofoams by Continuity Inversion of Dispersion* (NF-CID) principle [13, 14]. While the former suffers from the coarsening of the microemulsion structure [15], the latter avoids this weakness. In a new alternative approach, nanoporous polymer materials with an adjustable pore size between 80 and 800 nm were generated without a blowing agent at ambient conditions [16]. Starting from a crosslinked polymer gel, swollen with a mixture of at least two specially selected solvents, the nanoporous material was obtained from sequential evaporation of the solvents. However, in this work, the NF-CID principle was used to prepare polymeric nanofoams as tailor-made templates for the synthesis of highly porous organic/inorganic hybrid materials. The main advantages of the NF-CID principle, which is schematically shown in Fig. 1 and described in detail in the "Experimental section/methods", are the rapid saturation of a thermoplastic polymer with a

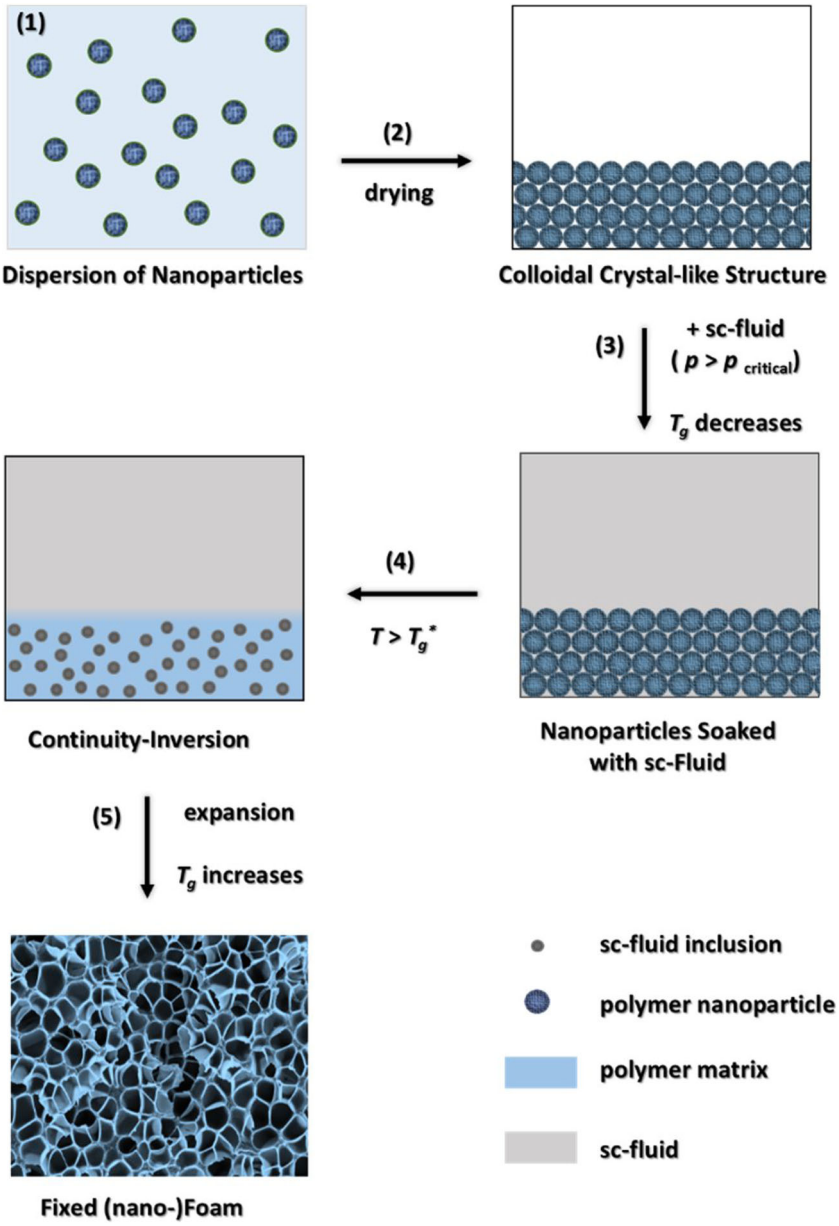

Fig. 1 Scheme of the NF-CID principle. (1) Thermoplastic nanoparticles synthesized by emulsion, miniemulsion, or microemulsion polymerization. (2) Drying the dispersion results in closed packed nanoparticles, which are in step (3) filled with a sc-fluid, decreasing the T_g of the polymer. (4) Increasing the temperature above the lowered T_g^*, the octahedral and tetrahedral voids (ideal packing) filled with the sc-fluid transform into spherical nanodroplets in the highly viscous polymer matrix. (5) Expanding the system leads to both foaming and fixation of the polymer. Redrawn from [13]

supercritical blowing agent and the high number density of supercritical blowing agent pools, both obtained by the use of polymer nanoparticles.

ZnO, as a semiconductor with tunable optical properties and potential applications in catalysis, photovoltaic, optoelectronic, etc., has been synthesized in confined spaces, where the pore size of the host matrix defines the shape and size of the obtained nanoparticles. Thus, nanocrystalline, size-selected ZnO was deposited inside the pores of a "wormhole" mesoporous silica [17], and applying an organometallic route ZnO species were hosted in the matrix of MCM-48 [18]. Furthermore, ZnO nanoparticles confined in mesoporous carbon [19] and zeolites [20] were synthesized. In contrast to the described above suspended in solution ZnO/host matrix nanocomposites, biotemplated three-dimensional ZnO nanonetworks [21], macroporous foams [22], foams with string-beaded morphology [23], nanotubes within the nanochannels of porous anodic alumina templates [24], and densely packed ZnO nanowires in confined space [25] were produced as well.

The goal of this work is to use polymer nanofoams as templates for the synthesis of three-dimensional nanoporous organic/inorganic hybrid materials. Thus, in the first part of this work, polystyrene (PS) nanoparticles are synthesized by emulsion polymerization and dried via isothermal ($T = 20$ °C) evaporation of the solvent (water) leading to a colloidal crystal-like close-packed arrangement of PS nanoparticles. Subsequently, these colloidal crystal-like structures were further processed following the NF-CID principle. The influence of temperature, exposure time, and the expansion process on the foam features was studied to adjust the pore diameter, polydispersity, and foam morphology. In the second part of this work, chemical bath deposition was used to mineralize PS foams with a pore size of 1 μm in order to form a metal oxide layer on the pore walls. Scanning electron microscopy (SEM), energy-dispersive X-ray (EDX), and uniaxial compression measurements were used to study the properties of this new nanoporous PS/ZnO hybrid material.

Experimental section/methods

In this section, the NF-CID principle, the synthesis of PS nanoparticles, the foaming of the colloidal crystal consisting of the close-packed PS nanoparticles, as well as the mineralization of PS foam are described. Furthermore, this section contains a brief description of the methods used for the characterization of the produced nanomaterials, i.e., SEM, dynamic light scattering (DLS), and uniaxial compression measurements.

Nanofoams by Continuity Inversion of Dispersion procedure

The principle can be divided in five steps: Firstly, thermoplastic polymer nanoparticles of adjustable size ($d_{part} \geq 10$ nm) and narrow size distribution are synthesized by emulsion [26], miniemulsion [27], or microemulsion [28, 29] polymerization. Hereafter, the nanoparticle dispersion is dried by evaporation of the solvent (step 2). Eventually, a colloidal crystal consisting of close-packed nanoparticles is formed. In step 3, the voids between the particles are filled with a supercritical fluid (sc-fluid) at an adjustable temperature and pressure. Because of the small size of the nanoparticles and the huge surface area of the colloidal crystal, the sc-fluid molecules, which later on act as blowing agent, diffuse almost instantaneously into the polymer nanoparticles. Time-resolved small angle neutron scattering (SANS) measurements showed that saturation times of the order of only 30 s are required [30].

Due to the saturation of the polymer nanoparticles with the sc-fluid, the glass temperature T_g is considerably reduced. Thereby, the lowered glass temperature T_g^* depends strongly on the solubility of a given sc-fluid in the polymer, which is a function of temperature and pressure [31]. For instance, PMMA which exhibits a glass temperature T_g of 105 °C transfers to the rubbery state already at $T = 40$ °C, if it is exposed to CO_2 adjusting a pressure of $p \geq 60$ bar [32].

In step 4 (continuity inversion), the temperature is increased above the T_g^* of the polymer nanoparticles saturated with the sc-fluid at the respective pressure. Thus, the polymer particles lose their spherical shape and form a connected polymer matrix. Due to the high interfacial tension between the sc-fluid and the saturated nanoparticles, the octahedral and tetrahedral voids (ideal packing) filled with sc-fluid transform to spherical nanodroplets in the highly viscous polymer matrix to minimize the interfacial energy. In the last step, the pressure is released to 1 bar. Thereby, the density of the sc-fluid changes gently from the liquid-like to a gas-like state. Accordingly, each spherical nanodroplet transforms gradually into a foam bubble. At the same time, the polymer matrix solidifies due to a rapid increase of T_g of the polymer to its original value, caused by the diffusion of sc-fluid molecules out of the polymer.

Assuming a spherical geometry, the diameter $d_{scfluid}$ of the spherical nanodroplets in the highly viscous matrix is directly related to the diameter d_{part} of the polymer nanoparticles, according to:

$$d_{scfluid} = d_{part} \sqrt[3]{\frac{N_{part}\phi_{scfluid}}{N_{scfluid}(1-\phi_{scfluid})}}. \quad (1)$$

Here, $\phi_{scfluid}$ is the volume faction of the sc-fluid and N_{part} and $N_{scfluid}$ are the number of particles and spherical nanodroplets, respectively. The volume of the spherical

nanodroplets and foam pores depends on the density of the sc-fluid at high and low pressure (1 bar), i.e., $\rho_{\text{scfluid,liquid-like}}$ and $\rho_{\text{scfluid,gas-like}}$, respectively. Thus, the diameter d_{pore} of a pore is given by:

$$d_{\text{pore}} = d_{\text{scfluid}} \sqrt[3]{\frac{\rho_{\text{scfluid,liquid-like}}}{\rho_{\text{scfluid,gas-like}}}} = d_{\text{part}} \sqrt[3]{\frac{\rho_{\text{scfluid,liquid-like}} N_{\text{part}} \phi_{\text{scfluid}}}{\rho_{\text{scfluid,gas-like}} N_{\text{scfluid}} (1-\phi_{\text{scfluid}})}}. \quad (2)$$

Altogether, this leads to the conclusion that the pore size in the foam is directly adjustable by the diameter of the used polymer nanoparticles. Assuming that the particles are ideally close-packed and that the octahedral and tetrahedral spaces are so close together that they build one inclusion when the polymer becomes ductile, $N_{\text{part}}/N_{\text{scfluid}} = 1$ and $\phi_{\text{scfluid}} \approx 0.26$. Calculating the diameter of a pore using CO_2 as sc-fluid and an expansion from $p = 250$ bar to 1 bar at 80 °C results in $d_{\text{pore}} \approx 5.4 \cdot d_{\text{part}}$.

From the discussion above, it is obvious that the diameter d_{part} of the polymer nanoparticles is one important parameter to adjust the pore size d_{pore} of the nanofoam. Besides d_{part}, the course of the NF-CID procedure has a comparable impact on the pore size, geometry, and homogeneity of the nanofoam. Particularly, the formation of sc-fluid filled nanodroplets in the highly viscous polymer matrix, i.e., continuity inversion (step 4), and the pressure release (step 5) are crucial steps for the procedure. Both are sensible to a coarsening of the structure via Ostwald ripening [33, 34] and coagulation followed by coalescence [35, 36], which is triggered by the minimization of the interfacial energy via a reduction of the interfacial area. Obviously, these aging phenomena depend strongly on the viscosity of the polymer matrix, which is controlled by the glass temperature T_g^* of the polymer saturated with the sc-fluid, temperature, pressure, exposure, and expansion time.

Nanoparticle synthesis

The polystyrene nanoparticle dispersions were synthesized via emulsion polymerization. Therefore, 170 ml degassed bidistilled water, 0.18 mol styrene (99%, Sigma-Aldrich), and 3 mmol sodium dodecyl sulfate (SDS) (> 99%, Sigma-Aldrich) were stirred in a three-necked round bottom glass flask, under nitrogen atmosphere, equipped with a stirrer, a heater, and a reflux condenser and heated up to 80 °C. The polymerization was initiated by the addition of 0.93 mmol potassium peroxodisulfate (99%, Fluka) dissolved in 10 ml degassed bidistilled water and reacted for 5 h. Moreover, 0.92 mmol of the chain transfer agent 2-ethyl hexyl thioglycolate (> 95%, from Sigma-Aldrich) was added together with the monomer to the reaction mixture. The particle growth during the reaction was followed by DLS measurements. After 5 h, the dispersion was cooled down to room temperature and filtrated using filter paper with 4–12 μm particle retention. To form the colloidal crystals, the dispersion was left aside uncovered at room temperature for some days until the solvent was completely evaporated.

Foaming experiments

The foaming experiments were carried out in a batch process using an in-house built high-pressure sapphire cell [12]. The cell is equipped with a sapphire cylinder ($h = 50$ mm, $Ø_{\text{internal}} = 10$ mm, $Ø_{\text{external}} = 40$ mm) that allows to observe the entire sample volume of about 3 ml. Pressures up to $p = 400 \pm 5$ bar can be generated by turning a piston down into the sapphire cylinder. The pressure is measured by a miniature pressure transducer (Type 8530, Burster, Germany), placed in a casing at the bottom of the sample cell. In order to control the temperature with an accuracy of $\Delta T = \pm 0.02$ K, the whole pressure cell is placed in a thermostated water bath.

For the foaming experiments, the colloidal crystals were put on a sample holder in the high-pressure cell. After the cell was closed with the piston, it was filled with liquid CO_2 (at room temperature and 72 bar) through a valve. Then, the cell was transferred to the water bath to adjust the temperature. When thermal equilibrium was reached, the pressure was adjusted moving the piston accordingly. After a targeted time at this pressure and temperature (exposure time), the pressure was released opening the valve rapidly.

Foam mineralization

Stock solution preparation

Methanol stock solutions of $Zn(OOCCH_3)_2 \cdot 2\ H_2O$ (34 mM) Sigma-Aldrich, tetraethylammonium hydroxide (TEAOH) (75 mM) (Aldrich Chemistry), and polyvinylpyrrolidone (PVP) (21.7 mM) ($M_w = 10{,}000$, Lot no. BCBJ4889V) (Sigma-Aldrich) were prepared. One volume unit of the zinc acetate was mixed with one volume unit of PVP stock solution. Then, one volume unit of TEAOH stock solution was added dropwise by the use of a peristaltic pump at a flow rate of 1.04 mL min^{-1} under continuous stirring. Thus, a precursor solution with a ratio of $[PVP]/[Zn^{2+}]/[TEAOH] = 1:1:1$ and final concentrations of $[PVP] = 7.23$ mM, $[Zn^{2+}] = 11.34$ mM, and $[TEAOH] = 25$ mM were obtained. The precursor solution was always prepared freshly prior to use. The deposition solution was prepared by adding 2 vol% ultrapure water to the precursor solution resulting in a total volume of 3 ml.

ZnO mineralization

A polystyrene foam cube (approx. $5 \times 5 \times 5$ mm^3) was placed in the vessel with 3 ml deposition solution and let to infiltrate for 10 min. Then, the vessel was heated in an oil bath to 60 °C for 1.5 h (1 deposition cycle). Subsequently, the foam was thoroughly rinsed with methanol and left in methanol for 1 h under stirring. Before starting the next cycle, the foam piece was dried under inert gas stream and then placed in a fresh deposition solution for the next deposition cycle. After the last washing step, the ZnO mineralized foam was dried under vacuum for 3 h. A reference sample was prepared in parallel by heating a PS foam cube in methanol at 60 °C for 1.5 h.

Characterization

Scanning electron microscopy

Imaging of the PS nanoparticles crystals, the PS foams and PS/ZnO hybrid foams were conducted by a Zeiss Merlin SEM at 3 kV (PS nanoparticles at 10 kV). The PS foams were fractured in liquid nitrogen to generate a breaking edge of the sample, so that the internal structure could be investigated: To avoid charging of the sample, the fixation was performed using silver lacquer. Additionally, the PS samples were sputtered with 5.0 nm iridium, while the PS/ZnO hybrid foams were sputtered with 0.3 nm iridium. *SEM coupled with EDX* measurements was conducted on a Zeiss Ultra 55 microscope. Thereby, the EDX spectra were obtained with a nitrogen-cooled EDAX detector. The size distributions of the particle and pore diameter were determined by analyzing the SEM images using the image-processing program *ImageJ*. At least 150 pores were analyzed to obtain the size distributions which were then fitted with the Gauss distribution to calculate the mean pore diameter.

Dynamic light scattering

The PS nanoparticles were studied by DLS at 25 °C using a three-dimensional LS spectrometer (LS Instruments, Switzerland). Diluted samples of the nanoparticles were irradiated with coherent, monochromatic light of a helium/neon laser ($\lambda = 633$ nm). The scattering was measured at different angles ranging from 30° to 150° in intervals of 10°. To ensure the reproducibility of the results, all measurements were repeated three times. The intensity of the scattered light was detected by a photomultiplier and converted by a correlator into an intensity-time-autocorrelation function, which was analyzed using *CONTIN* [37].

Mechanical characterization

A BOSE ElectroForce 3200 Series III instrument, which is controlled via a WinTest7 control system and equipped with a load cell capable to bear 220 N, was used to perform uniaxial compression measurements on cubic samples of the generated polystyrene foams and PS/ZnO hybrid materials with a strain rate of $5.0 \cdot 10^{-3}$ mm/s and up to 70% compression.

Results and discussion

This part starts with the characterization of the polystyrene nanoparticle dispersions and the colloidal crystal-like close-packed arrangement of the particles by DLS and SEM. Subsequently, the influence of the NF-CID parameters temperature, exposure time and expansion on the pore diameter, polydispersity, and morphology of the foam is shown by SEM images. Then, SEM, EDX, and uniaxial compression studies of the mineralized PS foams elucidate the generation of a new nanoporous organic/inorganic hybrid material.

Characterization of polystyrene nanoparticles and their colloidal crystal-like arrangement

The first step of the NF-CID principle is the synthesis of PS nanoparticles. In the study at hand, emulsion polymerization was used (for details, see "Experimental section/methods" section). In order to determine the size and polydispersity of the PS nanoparticles, the dispersions were diluted with bidistilled water and studied with DLS at 25 °C. From the analysis of the recorded intensity-time-autocorrelation function with *CONTIN*, a hydrodynamic diameter of $d_h = 69 \pm 5$ nm was obtained. Drying the dispersion via isothermal ($T = 20$ °C) evaporation of water, a colloidal crystal-like material consisting of close-packed PS nanoparticles was formed (step 2). Characterizing this material by SEM (see Fig. 2), indeed a close-packed arrangement of PS nanoparticles can be observed. As can be seen, packing defects are also evident, which are mainly caused by the particle size polydispersity and the drying procedure. Analyzing the SEM images a particle diameter of $d = 48 \pm 6$ nm is found. The mismatch between the diameter determined with SEM and DLS can be explained by the fact that DLS measures the diffusion of the particles and their hydration shell (hydrodynamic diameter d_h), while the SEM image displays the physical diameter.

Generation of PS nanofoams using the NF-CID principle: influence of process parameters

Following the course of the NF-CID principle, in step 3, the high-pressure cell containing the colloidal crystal was filled with liquid CO_2 at an adjustable temperature and pressure.

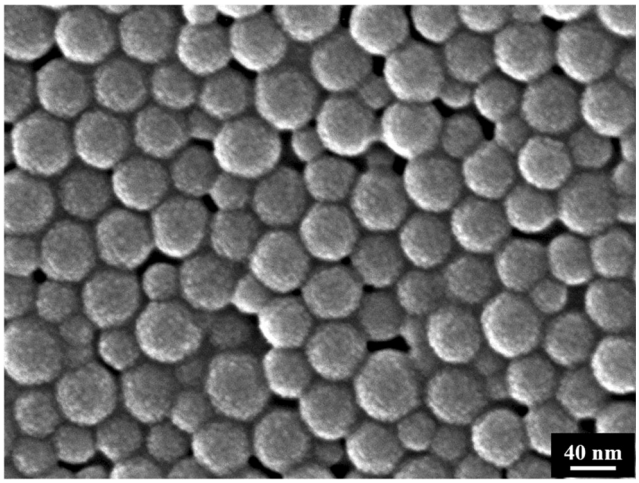

Fig. 2 SEM image of closely packed PS nanoparticles obtained via the synthesis of the nanoparticles by emulsion polymerization and isothermal ($T = 20$ °C) evaporation of the solvent (water). A close-packed arrangement of PS nanoparticles (of a diameter of 48 ± 6 nm) with some packing defects can be observed

Accordingly, the voids between the particles are filled with $scCO_2$. As a result of the small size of the nanoparticles and the huge surface area of the colloidal crystal, the polymer nanoparticles are very rapidly (30 s) saturated with CO_2, reducing the glass temperature T_g considerably. The next and most important step (4) of the NF-CID principle is the so-called continuity inversion. Adjusting the temperature above the lowered T_g^*, the polymer particles lose their spherical shape and form a connected polymer matrix. Due to the high interfacial tension between the sc-fluid and the saturated nanoparticles, the octahedral and tetrahedral voids (ideal packing) filled with sc-fluid transform to spherical nanodroplets in the highly viscous polymer matrix to minimize the interfacial energy. As the T_g^* depends not only on the average molecular weight of the polymer but also on the CO_2 solubility in the PS nanoparticles, the temperature and pressure, at which the continuity inversion takes place, have to be determined experimentally performing systematic foaming experiments.

In a first set of experiments, the influence of the temperature on the NF-CID process was studied using colloidal crystals of closely packed PS nanoparticles ($d = 48$ nm) (Fig. 2) adjusting a pressure of $p = 250$ bar. After an "exposure time" of 15 min, the pressure is released opening the valve rapidly. SEM images of the highly porous material obtained at five different temperatures ($T = 35$, 45, 55, 65, and 75 °C) are shown in Fig. 3. Performing the NF-CID process at $T =$ 35 °C, almost any pore can be seen in the PS bulk material, i.e., no foaming has taken place. Instead, in some areas of the SEM image, even the nanoparticles are still visible. This implies that at 35 °C, the T_g^* of the CO_2-loaded PS particles is not exceeded. Performing the same experiment at a temperature of 45 °C, nanopores in the PS matrix can be observed. These results suggest that at $T = 45$ °C, the T_g^* is reached, enabling the onset of the continuity inversion from closely packed PS nanoparticles-in-CO_2 to CO_2-nanodroplets-in a highly viscous PS polymer matrix. Analyzing the SEM images, a pore diameter of 274 ± 62 nm, porosity of 34%, and cell density of $5.3 \cdot 10^5$ cm^{-3} were found. However, the relatively low porosity and the low cell density indicate that the continuity inversion was most probably not fully completed.

Then, the NF-CID process was performed at $T = 55$ °C. As can be seen, a nanocellular foam with a diameter of 830 ± 200 nm, porosity of 49%, and cell density of $1.5 \cdot 10^{12}$ cm^{-3} was obtained, which implies that at 55 °C the T_g^* of the CO_2-loaded PS particles is exceeded so that the continuity inversion apparently has taken place.

Another two foaming experiments were performed at $T =$ 65 °C and $T = 75$ °C, keeping again the other parameters, i.e., particle diameter, pressure, and exposure time constant. As can be seen, performing the NF-CID process at $T = 65$ °C led to a PS foam with a larger pore diameter of 1.21 ± 0.28 μm, a porosity of 63%, and a cell density of $5.3 \cdot 10^{11}$ cm^{-3}. The increase of the pore diameter (compared to the foaming experiment at $T = 55$ °C) becomes explainable taking into account the lower viscosity of the PS matrix at $T = 65$ °C. Aging processes as the Ostwald ripening [33, 34] of the CO_2 nanodroplets as well as their coagulation and coalescence [35, 36] lead to larger CO_2 droplets and as a consequence to larger pores. Interestingly, the foaming experiment performed at a further increased temperature of $T = 75$ °C led to a bimodal cell morphology with even larger pore diameters of 13 and 4.5 μm. Imaging the foam structure with a smaller magnification (not shown), it becomes obvious that the larger pores are formed preferentially along the grain boundaries of the colloidal crystals.

Summarizing the results of the foaming experiments performed adjusting the same closely packed PS nanoparticles ($d = 48$ nm) at a pressure of 250 bar, and an exposure time of 15 min but varying the temperature, it can be concluded that the onset of foaming was obtained at 45 °C. Increasing the temperature by 10 K, the colloidal crystal of closely packed PS nanoparticles was evenly foamed. However, the foaming experiments performed at 65 and 75 °C suggest that also the foam obtained at 55 °C suffers from a coarsening of the structure.

In order to study whether coarsening has taken place at 55 °C, the exposure time was increased to 30 min keeping the other parameters of the NF-CID procedure constant. Figure 4 shows the recorded SEM images of both foaming experiments in direct comparison. As can be seen, the size of the pores increases with increasing exposure time, confirming the assumption that coarsening processes are already present at 55 °C. Analyzing the SEM images, an increase of the pore diameter from 830 ± 200 to 1700 ± 500 nm was observed by increasing the exposure time from 15 min (left) to 30 min (right). Considering the image taken from the foam with $t =$

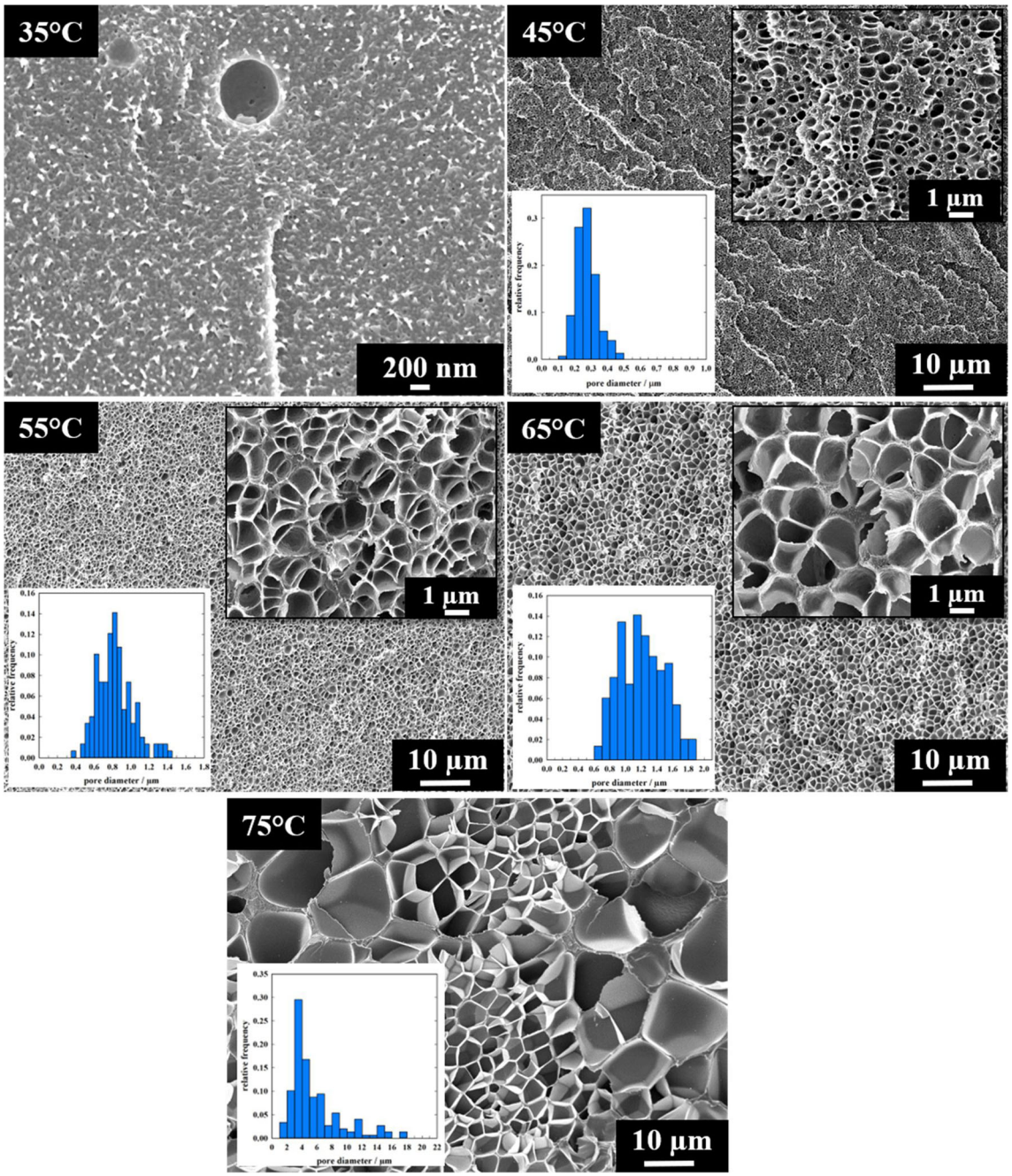

Fig. 3 SEM images of PS foams obtained via the NF-CID process at various temperatures. Colloidal crystals (Fig. 2) of closely packed PS nanoparticles ($d = 48$ nm) were filled with $scCO_2$ at $p = 250$ bar and $T = 35$, 45, 55, 65, as well as 75 °C. After an "exposure time" of 15 min, the pressure was released rapidly at the respective temperature. While no foaming of the slightly molten PS nanoparticles was observed at $T = 35$ °C, first pores exhibiting a diameter of 274 ± 62 nm were observed at $T = 45$ °C

30 min more closely, it becomes obvious that the foam consists of big plateau borders, while the cell membranes are thin. However, no windows can be observed in the cell membrane characterizing a closed cell foam. These findings indicate that the coarsening is a consequence of an Ostwald ripening [33, 34] of the CO_2 nanodroplets as well as their coagulation and coalescence [35, 36] rather than an expansion-induced coarsening.

The results so far show that the NF-CID parameters temperature and exposure time have a strong and systematic influence not only on the size d_{pore} and polydispersity of the pores but also on the overall structure of the nanofoam. With the goal to identify other important parameters of the principle, which have an impact on the properties of the nanofoam, we studied the influence of the course of the expansion process, starting again from the colloidal crystals of closely

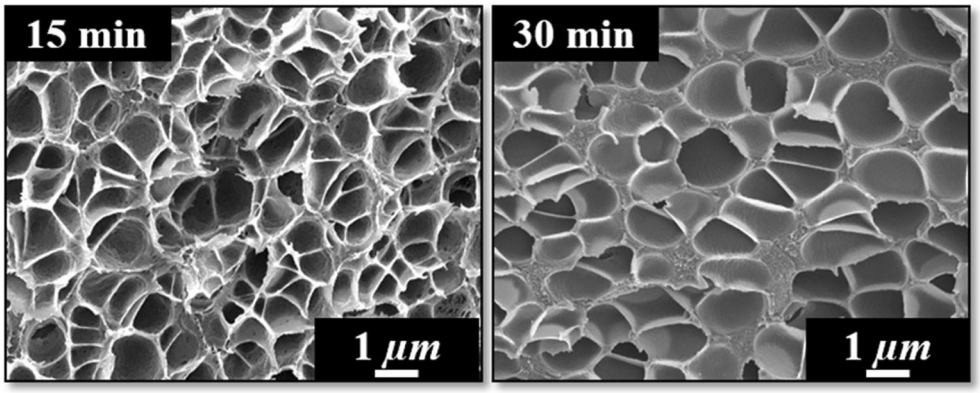

Fig. 4 SEM images of PS foams obtained via the NF-CID process applying different exposure times. Colloidal crystals of closely packed PS nanoparticles (d = 48 nm) (Fig. 2) were filled with $scCO_2$ at p = 250 bar and T = 55 °C. Increasing the exposure time from 15 min (left) to 30 min (right) led to an increase of the mean pore diameter from 830 ± 200 to 1700 ± 500 nm

packed PS nanoparticles (d = 48 nm) shown in Fig. 2. The CO_2 was added adjusting the temperature to 80 °C and the pressure to 250 bar. After an exposure time of 10 min, the temperature was decreased to 25 °C before the expansion. Due to the fact that the volume of the pressure cell was kept constant, the pressure decreased to 75 bar. Subsequently, the pressure was released to 1 bar.

The SEM images, shown in Fig. 5, show the obtained PS nanofoam, which seems to have a homogeneous open-cellular structure with a mean pore diameter of 65 nm, a cell density of $1 \cdot 10^{15}$ cm^{-3}, and a porosity of 47%. Comparing the pore diameter of the resulting material with the particle diameter (d_{part} = 48 ± 6 nm), it becomes obvious that the nanofoam is almost one to one copy of the template with regard to the length scales. One may speculate that the structure of the nanofoam is mainly formed and stabilized during the cooling step. In order to confirm this hypothesis, a time-resolved SANS study is planned.

Synthesis of PS/ZnO hybrid foams

The previous results nicely show that the NF-CID principle can be used to synthesize PS nanofoams with an adjustable pore size (d_{pore} > 65 nm) and polydispersity but also with tunable morphology. In the next step, we used these PS nanofoams for the synthesis of a new class of highly porous organic/inorganic hybrid materials, which was the main goal of this work. We selected a PS foam of a rather large pore diameter of 1.21 ± 0.28 µm obtained via the NF-CID process (colloidal crystals (Fig. 2) of closely packed PS nanoparticles (d = 48 nm), p = 250 bar, T = 65 °C, and t = 15 min), as a test bed to study the ability of the polymer foam to mineralize ZnO on the pore walls. The reaction was conducted under the mild reaction conditions of CBD. The procedure used for the ZnO deposition, described elsewhere [38], consists briefly in the following: Zinc acetate dihydrate, used as a zinc source, was hydrolyzed slowly in a methanol solution at slightly elevated temperature (60 °C), and ZnO nanoparticles were formed. The mineralization was performed in presence of the base TEAOH, needed to stabilize the pH, while PVP is used as structure-directing agent to control the size of ZnO particles within the nanometer range.

A cube of the PS foam was placed in the deposition solution, and the foam walls were used as a support and template to form a ZnO layer on top of it. In order to get a thicker inorganic film onto the pore walls, the solution was refreshed

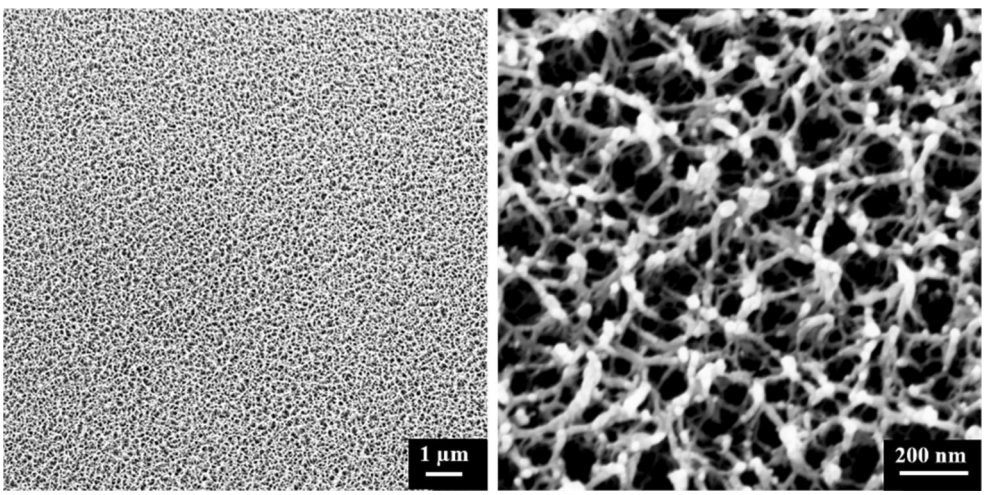

Fig. 5 SEM image of a PS nanofoam obtained from colloidal crystals of closely packed PS nanoparticles (d = 48 nm) filled with $scCO_2$ at p = 250 bar and T = 80 °C. After an exposure time of 10 min, the temperature was decreased to 25 °C entailing a pressure of p = 75 bar. Subsequently, the pressure was released to 1 bar resulting in an open-cellular foam exhibiting a mean pore diameter of 65 nm

after 1.5 h (1 deposition cycle), because after this time, agglomeration processes start to dominate over the particle formation [39]. As can be seen in the SEM image (Fig. 6b), the morphology of the initial PS foam (Fig. 6a) is preserved after 10 ZnO deposition cycles, and a thin inorganic film (approx. 50 nm) on the pore walls (approx. 200 nm) is observed. The top inset in (Fig. 6b) clearly shows the smooth polymer walls and the granular ZnO film. The chemical composition analysis by SEM/EDX (Fig. 6c) confirms the deposition of ZnO on the walls. As the ZnO layers are considerably thinner than the penetration depth of the electrons (ca. ~ 500 nm), the carbon signal observed in the EDX spectrum correlates to the underlying polymer substrate. Furthermore, since the applied mineralization approach allows for a precise control of the inorganic film thickness within several nanometers, the diameter of the pores can also be finely tuned by varying the number of the deposited cycles.

The successful mineralization of the PS foam points to the conclusion that the polymer pore walls should be charged (requirement for inorganic film formation). However, due to the absence of charged functional groups in the styrene monomer, the pore wall surface should be hydrophobic. This apparent contradiction resolves considering the method used for the synthesis of the PS particles. In emulsion polymerization, SDS is added as an emulsifier for micelle formation. During the polymerization, the hydrophobic tails of SDS are fixed in the polymerized polystyrene particles pointing their polar head outwards. When the colloidal crystals of closely packed PS nanoparticles are foamed, the sulfate groups become a part of the pore walls making them polar and appropriate for mineralization without need of further hydrophilization post-treatment steps (e.g., O_2-plasma).

Mechanical properties of bare PS foams and PS/ZnO hybrid foams

The mechanical properties of the bare PS and the PS/ZnO hybrid foams, shown in Fig. 6, have also been investigated by carrying out uniaxial compression studies. The obtained stress/strain curves are shown in Fig. 7. Both materials show a behavior which is known for solid foams [40]. Thus, the curves can be divided in two regimes, i.e., the linear-elastic regime (due to the cell wall bending) and the plateau regime of deformation (controlled by the elastic buckling and subsequent failure of the cell walls). Analyzing the stress/strain curves, an elastic modulus of $E_{\mathrm{PS\ foam}} = 26.7$ MPa and a yield stress of 1.20 MPa were found for pure PS foam (blue), while larger values of $E_{\mathrm{PS/ZnO}} = 37.4$ and 1.75 MPa were found for the porous PS/ZnO hybrid, as expected due to the presence of the ZnO layer.

The value found for the yield stress of the pure PS foam can be compared to the data for PS foams found in literature.

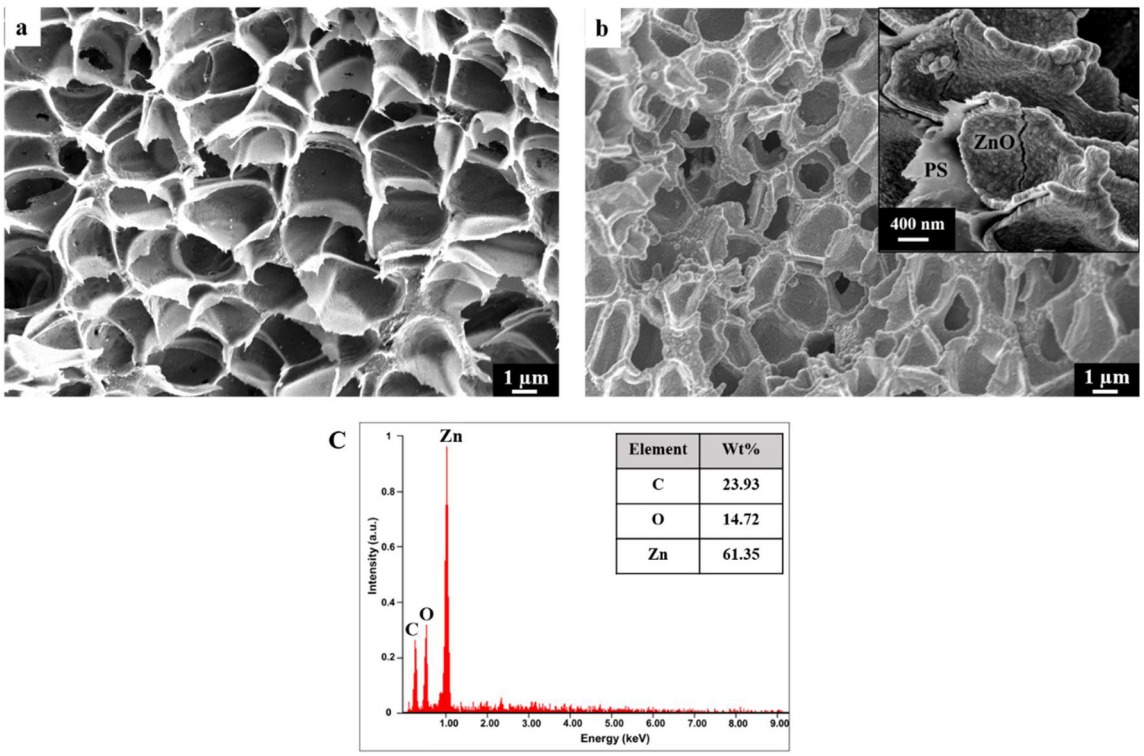

Fig. 6 **a** SEM image of a PS foam obtained from colloidal crystals of closely packed PS nanoparticles ($d = 48$ nm) filled with $scCO_2$ at $p =$ 250 bar, $T = 65$ °C, and an exposure time of 15 min. **b** SEM image of the porous PS/ZnO hybrid material obtained after 10 ZnO deposition cycles. The upper inset represents ZnO mineralized pores showing smooth polymer walls and the granular ZnO film. **c** EDX elemental analysis of porous PS/ZnO hybrid, which confirms the mineralization of PS foams

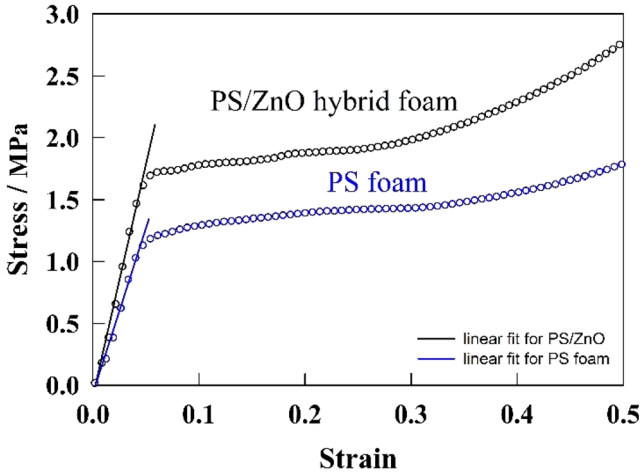

Fig. 7 Stress/strain curves of the pure PS foam (blue) and the porous PS/ZnO hybrid material (black) (shown in Fig. 6) obtained by uniaxial compression studies. An elastic modulus of $E_{\mathrm{PS\ foam}} = 26.7$ MPa and a critical stress of 1.20 MPa is found for pure PS foam (blue), while larger values of $E_{\mathrm{PS/ZnO}} = 37.4$ and 1.75 MPa are found for the porous PS/ZnO hybrid material, as expected due to the presence of the ZnO layer

Arora et al. [41] could show that the yield stress of polystyrene foams decreases with decreasing pore size and density of the foam. Studying a PS foam with a pore size of 5 μm and a density of 0.3 g cm^{-3}, they found a critical stress of 11.1 MPa, which is one order of magnitude larger than our PS foam under study. However, the PS foams presented here have a smaller pore diameter of 1.21 ± 0.28 μm and an expected lower density. Therefore, the obtained lower yield stress is in a good agreement with the trends discussed by Arora et al. [41].

Conclusion

In this study, PS nanofoams were utilized for the synthesis of porous organic/inorganic hybrid materials, which are potential candidates for a wide range of applications such as sorption, sensing, and catalysis. Following the NF-CID principle, we were able to produce PS nanofoams with an adjustable pore size ($d_{\mathrm{pore}} > 65$ nm), polydispersity, and tunable morphology. Therefore, we synthesized PS nanoparticles with a radius of $d = 48 \pm 6$ nm via emulsion polymerization. Gentle drying of the dispersion led to the formation of a colloidal crystal-like material consisting of close-packed polystyrene nanoparticles.

In order to be able to adjust the pore diameter, polydispersity, and foam morphology, the influence of important parameters of the NF-CID process was studied. Investigating the influence of the temperature, the experiments revealed the onset of foaming at a temperature of 45 °C yielding a pore diameter of 274 ± 62 nm (Fig. 3). Increasing the temperature by 10 K, the colloidal crystal turned out to be evenly foamed exhibiting a pore diameter of 830 ± 200 nm. A further increase of the temperature to 65 and 75 °C led to a further increase of the pore diameter due to Ostwald ripening of the CO_2 nanodroplets as well as their coagulation and coalescence. The study of the influence of the exposure time confirmed that adjusting a temperature above the glass temperature T_g^* of the polymer nanoparticles saturated with the sc-fluid, the PS foam structure suffers strongly from coarsening processes (Fig. 4). That the course of the expansion process has a strong influence on the foam structure could be shown by filling the colloidal crystal at $p = 250$ bar and $T = 80$ °C and decreasing the temperature to 25 °C entailing a pressure of 75 bar after an exposure time of 10 min. Releasing the pressure only then to 1 bar led to formation of an open-cellular foam (Fig. 5) with a pore diameter of only 65 nm, which is only slightly larger than the size of the used PS nanoparticles.

In the second part of this work, we selected a PS foam exhibiting a rather large pore diameter of 1.21 ± 0.28 μm to infiltrate a mineralization solution containing the semiconducting ZnO using CBD. SEM coupled with EDX shows that the morphology of the initial PS foam is preserved after 10 deposition cycles, and a thin inorganic film on the pore walls is formed (Fig. 6). Thereby the success of the mineralization was attributed to the presence of SDS residues on the hydrophobic PS surface. Uniaxial compression studies (Fig. 7) of the bare PS and the PS/ZnO hybrid yielded larger values of E modulus and critical stress for the porous PS/ZnO hybrid material as expected due to the presence of the ZnO layer.

In summary, we synthesized for the first time (to our knowledge) a porous PS/ZnO material via the infiltration of a PS foam by a methanol precursor solution of semiconducting ZnO retaining the general structure of the PS foam. Furthermore, applying the NF-CID principle, we were able to adjust the underlying template structure of the PS foam with respect to pore size, polydispersity, and morphology. Last but not least, the applied mineralization approach allows for a precise control over the inorganic film thickness within several nanometers. Therewith, the diameter of the pores can also be finely tuned by varying the number of the deposited cycles.

Acknowledgements The authors thank Herbert Metzner (Workshop, University of Cologne, Germany) as well as Boris Tschertsche and Daniel Relovsky (Workshop, University Stuttgart, Germany) for the development and maintenance of the HP cells, respectively, as well as the scientific facility Nanostrukturlabor of J. Weis and the department of J. Spatz from the Max Planck Institutes in Stuttgart, Germany for their technical support and equipment access. Furthermore, Yaseen Qawasmi is grateful to the Konrad Adenauer Stiftung for the financial support.

Compliance with ethical standards

Conflict of interest The authors declare that they have no conflict of interest.

References

1. Sanchez C, Belleville P, Popall M, Nicole L (2011) Applications of advanced hybrid organic-inorganic nanomaterials: from laboratory to market. Chem Soc Rev 40:696–753. https://doi.org/10.1039/c0cs00136h
2. Weiner S, Dove PM (2003) An overview of biomineralization processes and the problem of the vital effect. Rev Mineral Geochem 54(1):1–29. https://doi.org/10.2113/0540001
3. Stephens CJ, Ladden SF, Meldrum FC, Christenson HK (2010) Amorphous calcium carbonate is stabilized in confinement. Adv Funct Mater 20:2108–2115. https://doi.org/10.1002/adfm.201000248
4. Knudsen M (1909) Eine Revision der Gleichgewichtsbedingung der Gase. Thermische Molekularströmung. Ann Phys 336:205–229
5. Jelle BP, Gustavsen A, Baetens R (2010) The path to the high performance thermal building insulation materials and solutions of tomorrow. J Build Phys 34(2):99–123. https://doi.org/10.1177/1744259110372782
6. Kistler SS (1931) Coherent expanded aerogels and jellies. Nature 127:741
7. Reichenauer G, Heinemann U, Ebert HP (2007) Relationship between pore size and the gas pressure dependence of the gaseous thermal conductivity. Colloids Surf A Physicochem Eng Asp 300:204–210. https://doi.org/10.1016/j.colsurfa.2007.01.020
8. Krause B, Sijbesma HJP, Mu P (2001) Bicontinuous nanoporous polymers by carbon dioxide foaming. Macromolecules 34(25):8792–8801
9. Siripurapu S, Coughlan JA, Spontak RJ, Khan SA (2004) Surface constrained foaming of polymer thin films with supercritical carbon dioxide. Macromolecules 37(26):9872–9879
10. Butler R, Davies CM, Cooper I (2001) Emulsion templating using high internal phase supercritical fluid emulsions. Adv Mater 13:1459–1463
11. Strey R, Sottmann T, Schwan M (2008) Aufgeschäumtes Material und Herstellungs-verfahren für das aufgeschäumte Material. DE10260815B4
12. Schwan M, Kramer L, Sottmann T, Strey R (2010) Phase behaviour of propane- and scCO2-microemulsions and their prominent role for the recently proposed foaming procedure POSME (Principle of Supercritical Microemulsion Expansion). Phys Chem Chem Phys 12:6247–6252
13. Strey R, Müller A (2010) Erzeugung nanodisperser Einschlüsse in einer hochviskosen Matrix. DE102010053064A1
14. Müller A (2013) Preperation of polymer nano-foams: templates, challenges, and kinetics. (PhD Thesis, University of Cologne), Cuvillier Verlag, ISBN: 978-3-95404-566-2, Cologne
15. Müller A, Pütz Y, Oberhoffer R, Becker N, Strey R, Wiedenmann A, Sottmann T (2014) Kinetics of pressure induced structural changes in super- or near-critical CO_2-microemulsions. Phys Chem Chem Phys 16:18092–18097. https://doi.org/10.1039/C3CP53790K
16. Grassberger L, Koch K, Oberhoffer R, Müller A, Klemmer HFM, Strey R (2017) Blowing agent free generation of nanoporous poly(methylmethacrylate) materials. Colloid Polym Sci 295:379–389. https://doi.org/10.1007/s00396-017-4012-1
17. Polarz S, Neues F, van den Berg MWE, Grunert W, Khodeir L (2005) Mesosynthesis of ZnO-silica composites for methanol nanocatalysis. JACS 127(34):12028–12034. https://doi.org/10.1021/ja0516514
18. Schroder F, Hermes S, Parala H, Hikov T, Muhler M, Fischer RA (2006) Non aqueous loading of the mesoporous siliceous MCM-48 matrix with ZnO: a comparison of solution, liquid and gas-phase infiltration using diethyl zinc as organometallic precursor. J Mater Chem 16(35):3565–3574. https://doi.org/10.1039/B606814F
19. Suryavanshi U, Iijima T, Hayashi A, Hayashi Y, Tanemura M (2012) Fabrication of ZnO nanoparticles confined in the channels of mesoporous carbon. Chem Eng J 179:388–393. https://doi.org/10.1016/j.cej.2011.10.087
20. Shi JY, Chen J, Feng ZC, Chen T, Wang XL, Ying PL, Li C (2006) Time-resolved photoluminescence characteristics of subnanometer ZnO clusters confined in the micropores of zeolites. J Phys Chem B 110(51):25612–25618. https://doi.org/10.1021/jp060439z
21. Ceylan H, Ozgit-Akgun C, Erkal TS, Donmez I, Garifullin R, Tekinay AB, Usta H, Biyikli N, Guler MO (2013) Size-controlled conformal nanofabrication of biotemplated three-dimensional TiO_2 and ZnO nanonetworks. Sci Rep 3(2306):1–7 https://www.nature.com/articles/srep02306
22. Kovacic S, Anzlovar A, Erjavec B, Kapun G, Matsko NB, Zigon M, Zagar E, Pintar A, Slugovc C (2014) Macroporous ZnO foams by high internal phase emulsion technique: synthesis and catalytic activity. ACS Appl Mater Interfaces 6(21):19075–19081. https://doi.org/10.1021/am5050482
23. Wang PP, Zhao J, Xuan RF, Wang Y, Zou C, Zhang ZQ, Wan YZ, Xu Y (2014) Flexible and monolithic zinc oxide bionanocomposite foams by a bacterial cellulose mediated approach for antibacterial applications. Dalton Trans 43(18):6762–6768. https://doi.org/10.1039/c3dt52858h
24. Seo BI, Shaislamov UA, Ha MH, Kim SW, Kim HK, Yang B (2007) ZnO nanotubes by template wetting process. Physica E 37:241–244. https://doi.org/10.1016/j.physe.2006.07.025
25. Ladanov M, Algarin-Amaris P, Matthews G, Ram M, Thomas S, Kumar A, Wang J (2013) Microfluidic hydrothermal growth of ZnO nanowires over high aspect ratio microstructures. Nanotechnology 24(37):375301. https://doi.org/10.1088/0957-4484/24/37/375301
26. Hansen FK, Ugelstad J (1982) In: Piirma I (ed) Particle formation mechanisms in emulsion polymerization. Academic Press, New York, pp 51–91
27. Landfester K (2009) Miniemulsion polymerization and the structure of polymer and hybrid nanoparticles. Angew Chem Int Ed 48(25):4488–4507
28. Antonietti M, Hentze HP (1997) Neuere Aspekte der Polymerisation in lyotropen Phasen und in Mikroemulsionen. Chem Ing Tech 69(3):369–373
29. Puig JE, Rabelero M (2016) Semicontinuous microemulsion polymerization. Curr Opin Colloid Interface Sci 25:83–88. https://doi.org/10.1016/j.cocis.2016.07.003
30. Grassberger L (2016) (PhD Thesis, University of Cologne), ISBN: 978-3-8439-2623-2
31. Shieh Y, Liu K (2002) Solubility of CO_2 in glassy PMMA and PS over a wide pressure range: the effect of carbonyl groups. J Polym Res 9(2):107–113
32. Condo PD, Johnston KP (1994) In situ measurement of the glass transition temperature of polymers with compressed fluid diluents. J Polym Sci B Polym Phys 32:523–533
33. Ostwald W (1900) Über die vermeintliche Isomerie des roten und gelben Quecksilberoxyds und die Oberflächenspannung fester Körper. Z Phys Chem 34:495–503
34. Egelhaaf S, Olsson U, Schurtenberger P, Morris J, Wennerström H (1999) Quantitative measurements of Ostwald ripening using time-resolved small-angle neutron scattering. Phys Rev E 60:5681–5684
35. Smoluchowski M (1917) Mathematical theory of the kinetics of the coagulation of colloidal solutions. Z Phys Chem 19:129–135
36. Meakin P (1991) Steady state droplet coalescence. Physica A 171:1–18. https://doi.org/10.1016/0378-4371(91)90353-E
37. Provencher SW (1982) Contin: a constrained regularization method for inverting data represented by linear algebraic or integral equations. Comput Phys Commun 27(3):213–227
38. Atanasova P, Stitz N, Sanctis S, Maurer JHM, Hoffmann RC, Eiben S, Jeske H, Schneider JJ, Bill J (2015) Genetically improved monolayer-forming tobacco mosaic viruses to generate

nanostructured semiconducting bio/inorganic hybrids. Langmuir 31:3897–3903

39. Lipowsky P, Hoffmann RC, Welzel U, Bill J, Aldinger F (2007) Site-selective deposition of nanostructured ZnO thin films from solutions containing polyvinylpyrrolidone. Adv Funct Mater 17: 2151–2159
40. Gibson LJ (2005) Biomechanics of cellular solids. J Biomech 38: 377–399
41. Arora KA, Lesser AJ, McCarthy TJ (1998) Compressive behavior of microcellular polystyrene foams processed in supercritical carbon dioxide. Polym Eng Sci 38(12):2055–2062